Observability of the innermost stable circular orbit in a near-extremal Kerr black hole

Takahisa Igata[1,*] Keisuke Nakashi[1,†] and Kota Ogasawara[2,‡]

[1]*Department of Physics, Rikkyo University, Toshima, Tokyo 171-8501, Japan*
[2]*Theoretical Astrophysics Group, Department of Physics, Kyoto University, Kyoto 606-8502, Japan*

We consider the escape probability of a photon emitted from the innermost stable circular orbit (ISCO) of a rapidly rotating black hole. As an isotropically emitting light source on a circular orbit reduces its orbital radius, the escape probability of a photon emitted from it decreases monotonically. The escape probability evaluated at the ISCO also decreases monotonically as the black hole spin increases. When the dimensionless Kerr parameter a is at the Thorne limit $a = 0.998$, the escape probability from the ISCO is 58.8%. In the extremal case $a = 1$, even if the orbital radius of the light source is arbitrarily close to the ISCO radius, which coincides with the horizon radius, the escape probability remains at 54.6%. We also show that such photons that have escaped from the vicinity of the horizon reach infinity with sufficient energy to be potentially observed because Doppler blueshift due to relativistic beaming can overcome the gravitational redshift. Our findings indicate that signs of the near-horizon physics of a rapidly rotating black hole will be detectable on the edge of its shadow.

I. INTRODUCTION

The shadow structure of the M87 galactic center (M87*) discovered by the Event Horizon Telescope Collaboration [1–6] suggests that a supermassive black hole may exist there. However, the possibility that the center is a horizon-less compact object has not yet been ruled out [5,7,8]. If M87* is a black hole, while it is essential to observe the near-horizon region to distinguish it from black hole mimickers, because nothing can escape from the horizon, photons emitted from its vicinity seem unlikely to escape to infinity. Essentially, we can hardly perceive the scale of the gravitational radius of a black hole, and although we must continue to make observations to investigate physical phenomena at the horizon scale to identify the center, the simple perspective indicates the difficulty of further exploring the features of the central object.

However, according to recent research progress, this difficulty can be overcome. One of the targets that has an advantage in the observability of the near-horizon region is a rapidly rotating black hole. It has been shown that some observable features such as bright border of the shadow edge appear in a near-extremal Kerr black hole [9,10]; more recently, it was explicitly shown that in the extremal Kerr spacetime, the escape probability of a photon from a source at rest with respect to a locally nonrotating observer

is 29.1% in the limit as the emission point approaches the horizon [11,12].[1] Furthermore, the probability becomes zero in the same limit in the subextremal case, but in the near-extremal case, about 30% is still achieved just before the horizon. These facts suggest that the vicinity of a rapidly rotating black hole is more visible than that of a slowly rotating one. Because M87* is generally expected to have relatively high spin [14] and may be a rapidly rotating black hole [15,16], it is worth pursuing phenomena near the horizon of a near-extremal Kerr black hole.

In general, a light source near a black hole has proper motion relative to the horizon, which affects its photon escape probability and the initial energy injection to a photon. In particular, sources moving on stable circular orbits often exist in nature and further provide natural initial conditions for optically observable phenomena [17,18]. For instance, the apparent shape of the innermost edge of a standard accretion disk surrounding a black hole appears as a closed curve [19–24]. Since the innermost edge of an accretion disk is often identified with the innermost stable circular orbit (ISCO) [25], it is important to reveal whether or not photons emitted from the ISCO can reach infinity with sufficient energy to be observed. In particular, the ISCO radius coincides with the horizon radius in the extremal Kerr spacetime [26,27], so that the observability of the ISCO in a rapidly rotating black hole immediately implies that of the near-horizon region. The appearance of

---

*igata@rikkyo.ac.jp
†nakashi@rikkyo.ac.jp
‡kota@tap.scphys.kyoto-u.ac.jp

[1]Ratio of photons trapped by a black hole was also discussed in Ref. [13].

an isotropically emitting point source on a circular orbit in the near horizon of a rapidly rotating black hole has been investigated [28,29], and it was clarified that the point source moves on the so-called NHEKline on the photon ring.

One of the additional and specific features of a source on a stable circular orbit in the extremal Kerr spacetime is that, as its orbital radius approaches the ISCO (i.e., the horizon), the relative velocity to the extremal horizon increases and can get arbitrarily close to half of the speed of light [26]. Emission from this yields the boost of each photon and photon concentration in the forward direction of the source by the relativistic beaming. Therefore, it can be expected that the escape probability of a photon emitted from the ISCO of a rapidly rotating black hole becomes relatively large owing to the boost effect.

Understanding this phenomenon is important for observing certain features in the vicinity of the horizon. The purpose of this paper is to clarify how many photons emitted from a light source circularly orbiting a black hole can escape to infinity. In particular, when evaluating the escape probability of a photon from the ISCO in (near) extremal Kerr spacetimes, we demonstrate the possibility of observing the vicinity of the horizon from a distance. Furthermore, we also discuss the frequency shift of photons to confirm whether such photons reach infinity with sufficient energy.

This paper is organized as follows. In Sec. II, we derive the conditions for photon escape from the vicinity of the Kerr black hole horizon to infinity. In Sec. III, by using the results in the previous section, we define and show the escape cone of a photon emitted from a light source orbiting a black hole. Furthermore, we evaluate the escape probability under the assumption that the emission is isotropic. We also discuss the redshift for a photon observed at infinity. In Sec. IV, we present a summary and discussions. Throughout this paper, we use units in which $G = 1$ and $c = 1$.

II. ESCAPE OF A PHOTON FROM THE VICINITY OF THE Kerr BLACK HOLE HORIZON

The Kerr metric in the Boyer-Lindquist coordinates is given by

$$g_{\mu\nu}dx^\mu dx^\nu = -\frac{\Sigma\Delta}{A}dt^2 + \frac{\Sigma}{\Delta}dr^2 + \Sigma d\theta^2$$
$$+ \frac{A}{\Sigma}\sin^2\theta\left[d\varphi - \frac{a(r^2 + a^2 - \Delta)}{A}dt\right]^2, \quad (1)$$

$$\Sigma = r^2 + a^2\cos^2\theta, \qquad \Delta = r^2 + a^2 - 2Mr,$$
$$A = (r^2 + a^2)^2 - \Delta a^2\sin^2\theta, \quad (2)$$

where M and a are mass and spin parameters, respectively. We assume $0 < a \leq M$ in order to focus on a rotating black hole spacetime. The event horizon is located at the radius

$r = r_{\rm h} = M + \sqrt{M^2 - a^2}$. If $a = M$, the metric describes the extremal Kerr black hole spacetime, where $r_{\rm h} = M$. In the following part, units in which $M = 1$ are used.

We consider photon motion in the Kerr black hole spacetime. Let k^a be a null geodesic tangent. Because the metric admits the Killing vectors $\partial/\partial t$ and $\partial/\partial\varphi$, a free photon has constants of motion $k_t = k_a(\partial/\partial t)^a$ and $k_\varphi = k_a(\partial/\partial\varphi)^a$. Furthermore, the metric also admits the Killing tensor,

$$K_{ab} = \Sigma^2(d\theta)_a(d\theta)_b + \sin^2\theta[(r^2 + a^2)(d\varphi)_a - a(dt)_a]$$
$$\times [(r^2 + a^2)(d\varphi)_b - a(dt)_b] - a^2\cos^2\theta g_{ab}, \quad (3)$$

such that a photon has a quadratic constant of motion in k^a given by

$$Q = K_{ab}k^a k^b - (k_\varphi + ak_t)^2. \quad (4)$$

We assume positivity of photon energy (i.e., $-k_t > 0$) because we only focus on photons reaching infinity. Here, we introduce the impact parameters,

$$b = -\frac{k_\varphi}{k_t}, \qquad q = \frac{Q}{k_t^2}. \quad (5)$$

Rescaling the tangent k^a by $-k_t$ (i.e., $-k^a/k_t \to k^a$), we rewrite the components of k^a in terms of b and q as follows:

$$k^t = \dot{t} = \frac{1}{\Sigma}\left[a(b - a\sin^2\theta) + \frac{r^2 + a^2}{\Delta}(r^2 + a^2 - ab)\right], \quad (6)$$

$$k^r = \dot{r} = \frac{\sigma_r}{\Sigma}\sqrt{R}, \quad (7)$$

$$k^\theta = \dot{\theta} = \frac{\sigma_\theta}{\Sigma}\sqrt{\Theta}, \quad (8)$$

$$k^\varphi = \dot{\varphi} = \frac{1}{\Sigma}\left[\frac{b}{\sin^2\theta} - a + \frac{a}{\Delta}(r^2 + a^2 - ab)\right], \quad (9)$$

where σ_r, $\sigma_\theta = \pm$, the dot denotes the derivative with respect to an affine parameter, and

$$R = (r^2 + a^2 - ab)^2 - \Delta[q + (b - a)^2], \quad (10)$$

$$\Theta = q - b^2\cot^2\theta + a^2\cos^2\theta. \quad (11)$$

We review conditions for a photon escaping from the vicinity of the horizon to infinity [12]. To derive them, we analyze the equation of photon radial motion (7), which is rewritten as

$$\dot{r}^2 + \frac{r(r-2)}{\Sigma^2}(b - b_1)(b - b_2) = 0, \quad (12)$$

where

$$b_1(r) = \frac{-2ar + [r\Delta(r^3 - qr + 2q)]^{1/2}}{r(r-2)}, \quad (13)$$

$$b_2(r) = \frac{-2ar - [r\Delta(r^3 - qr + 2q)]^{1/2}}{r(r-2)}. \quad (14)$$

We call b_i ($i = 1$, 2) the effective potentials for photon radial motion. The allowed parameter range of b for a positive energy photon is

$$b \le b_1 \quad \text{for } r_h < r < 2, \quad (15)$$

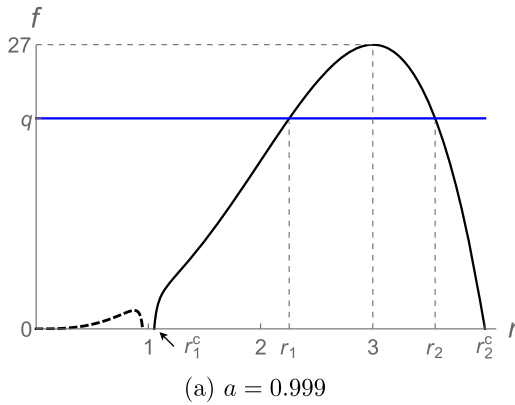$$b_2 \le b \le b_1 \quad \text{for } r \ge 2. \quad (16)$$

Since the escape of a photon is governed by the potential barrier, the extremum points of b_i ($i = 1, 2$) should be known. Solving $b_i'(r) = 0$ for q, we obtain a common equation

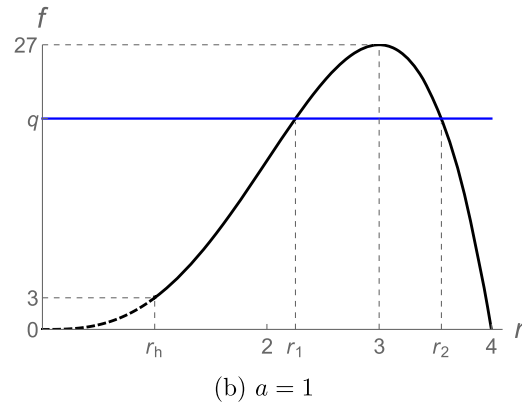$$q = f(r) \equiv \frac{r^2}{a^2}\left[-\frac{4(1-a^2)r}{(r-1)^2} + 3 + (3-r)(r-1)\right]. \quad (17)$$

It is sufficient to investigate the region where $f(r) \ge 0$ because the light source we discuss is located on the equatorial plane, and therefore, from Eqs. (8) and (11), a photon must initially satisfy $\Theta = q \ge 0$. Figure 1(a) shows a typical shape of $f(r)$ in the case of subextremal Kerr spacetimes (i.e., $0 < a < 1$). This figure shows that Eq. (17) has two roots r_1, r_2 outside the horizon, which are restricted in the range

$$r_h < r_1^c \le r_1 \le 3 \le r_2 \le r_2^c, \quad (18)$$

where $r = 3$ is a local maximum point of f, and

$$r_1^c = 2 + 2\cos\left[\frac{2}{3}\arccos(a) - \frac{2\pi}{3}\right], \quad (19)$$

$$r_2^c = 2 + 2\cos\left[\frac{2}{3}\arccos(a)\right] \quad (20)$$

are radii of circular photon orbits solving the equation $f = 0$ (i.e., $q = 0$). When a photon stays at the top of an extremum point of b_1 (b_2), the orbit with constant radius $r = r_1$ ($r = r_2$) is called the spherical photon orbit. Then the photon must have

$$b = b_i^s \equiv \frac{2(1-a^2)}{a(r_i - 1)} - \frac{(r_i - 1)^2}{a} + \frac{3}{a} - a. \quad (21)$$

Next, we focus on the case of the extremal Kerr spacetime (i.e., $a = 1$), for which the first term in f vanishes such that Eq. (17) reduces to

$$q = r^3(4 - r). \quad (22)$$

Figure 1(b) shows the shape of f in the extremal case (i.e., $a = 1$). Contrary to the subextremal case, the number of roots of Eq. (17) depends on q. Outside the horizon, there exists a single root r_2 for $0 \le q \le 3$, while there exist two roots r_1, r_2 outside the horizon for $3 < q < 27$, where the boundary values of the ranges come from $f(r_h) = 3$ and $f(3) = 27$.

Let us consider escape conditions for a photon in terms of (b, q). Classifying the radial position r of a light source based on relations with the extremum point r_1 and the horizon r_h, we clarify the parameter range of (b, q) for a photon that can escape from the vicinity of the horizon to infinity. In the following part, it is assumed that $r < 3$.

Case a.—We consider the case $r_1 < r_h < r$, which we define as Case a. Note that this inequality appears only for the extremal case because $r_1 > r_h$ always holds for the

(a) $a = 0.999$

(b) $a = 1$

FIG. 1.   Relation between the impact parameter q and the radii r_i ($i = 1, 2$) of extremum points of the effective potentials $b_i(r)$. The function f is shown by black lines, which are solid outside the horizon and dashed inside it. The left panel (a) is a subextremal case ($a = 0.999$), and the right panel (b) is the extremal case ($a = 1$).
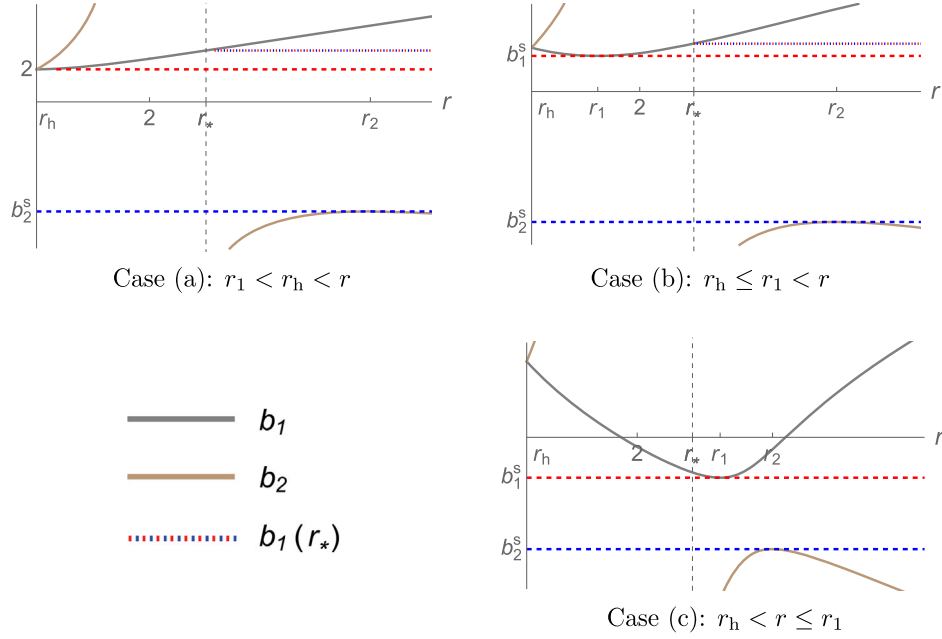
FIG. 2. Typical shapes of the effective potentials b_i ($i = 1, 2$) and parameter ranges of b for escaping photons. The radius r_* indicates the radial position of the source.

subextremal case [see Fig. 1 and Eq. (18)]. The first inequality $r_1 < r_h$ leads to $0 \leq q < 3$. In this range of q, we have typical plots of b_1, b_2 and marginal parameter values of b, as shown in Fig. 2(a). From this plot, the allowed range of b for escape can be read as follows: if $\sigma_r = +$ (i.e., radially outward emission), a photon with $b_2^s < b \leq b_1$ (i.e., the bounded range between the blue lines) can escape to infinity. Even if $\sigma_r = -$ (i.e., radially inward emission), a photon with $2 < b < b_1$ (i.e., the bounded range between the red lines) can do so. Hence, we find that the marginal parameter values of b are given by $(\sigma_r, b) = (+, b_2^s), (-, 2)$.

Case b.—We consider the case $r_h \leq r_1 < r$, which we define as Case b. The corresponding range of q is $3 \leq q < f$ for $a = 1$ and $0 \leq q < f$ for $0 < a < 1$. Figure 2(b)

shows typical plots of b_i in these ranges of q. If $\sigma_r = +$, a photon with $b_2^s < b \leq b_1$ (i.e., between the blue lines) can escape infinity, while if $\sigma_r = -$, a photon with $b_1^s < b < b_1$ (i.e., between the red lines) can do so. Hence, we find that marginal parameter values of b are given by $(\sigma_r, b) = (+, b_2^s), (-, b_1^s)$.

Case c.—We consider the case $r_h < r \leq r_1$, which we define as Case c. Then the parameter range of q is restricted to $f \leq q < 27$. Figure 2(c) shows typical plots of b_i in this ranges. Only if $\sigma_r = +$, a photon can escape to infinity, and it must then have $b_2^s < b < b_1^s$ (i.e., between the red and blue lines). Hence, we find that marginal parameter values b are given by $(\sigma_r, b) = (+, b_1^s), (+, b_2^s)$.

The allowed parameter values of (b, q) for escape from the vicinity of the horizon are summarized in Tables I and II.

TABLE I. ($a = 1$) Allowed parameter values of (b, q) for escape from the vicinity of the horizon in the extremal Kerr spacetime.

Cases	q	b ($\sigma_r = +$)	b ($\sigma_r = -$)	Marginal pairs of (σ_r, b)
(a) $r_1 < r_h < r$	$0 \leq q < 3$	$b_2^s < b \leq b_1$	$2 < b < b_1$	$(+, b_2^s)$ and $(-, 2)$
(b) $r_h \leq r_1 < r$	$3 \leq q < f$	$b_2^s < b \leq b_1$	$b_1^s < b < b_1$	$(+, b_2^s)$ and $(-, b_1^s)$
(c) $r_h < r \leq r_1$	$f \leq q < 27$	$b_2^s < b < b_1^s$	n/a	$(+, b_2^s)$ and $(+, b_1^s)$

TABLE II. ($0 < a < 1$) Allowed parameter values of (b, q) for escape from the vicinity of the horizon in a subextremal Kerr black hole spacetime.

Cases	q	b ($\sigma_r = +$)	b ($\sigma_r = -$)	Marginal pairs of (σ_r, b)
(b) $r_h \leq r_1 < r$	$0 \leq q < f$	$b_2^s < b \leq b_1$	$b_1^s < b < b_1$	$(+, b_2^s)$ and $(-, b_1^s)$
(c) $r_h < r \leq r_1$	$f \leq q < 27$	$b_2^s < b < b_1^s$	n/a	$(+, b_2^s)$ and $(+, b_1^s)$

III. ESCAPE CONE, ESCAPE PROBABILITY, AND REDSHIFT

We focus on a light source circularly orbiting a rotating black hole on the equatorial plane $\theta = \pi/2$. The energy E and angular momentum L of a source in a prograde circular orbit of radius r are given by [26]

$$E = \frac{r^{3/2} - 2r^{1/2} + a}{r^{3/4}(r^{3/2} - 3r^{1/2} + 2a)^{1/2}}, \qquad (23)$$

$$L = \frac{r^2 - 2ar^{1/2} + a^2}{r^{3/4}(r^{3/2} - 3r^{1/2} + 2a)^{1/2}}. \qquad (24)$$

We restrict the orbital radius r of the source in the range $r \geq r_\mathrm{I}$, where r_I is the ISCO radius,

$$r_\mathrm{I} = 3 + Z_2 - [(3 - Z_1)(3 + Z_1 + 2Z_2)]^{1/2}, \quad (25)$$

$$Z_1 = 1 + (1 - a^2)^{1/3}[(1 + a)^{1/3} + (1 - a)^{1/3}], \quad (26)$$

$$Z_2 = (3a^2 + Z_1^2)^{1/2}. \qquad (27)$$

Note that r_I approaches r_h as a approaches the extremal value 1. In the extremal case, r_I coincides with the horizon radius, i.e., $r_\mathrm{I} = r_\mathrm{h} = 1$.

To describe a photon emission from the source, we introduce a frame associated with its rest frame,

$$e^{(0)} = -E\mathrm{d}t + L\mathrm{d}\varphi, \qquad (28)$$

$$e^{(1)} = \frac{r}{\sqrt{\Delta}}\mathrm{d}r, \qquad (29)$$

$$e^{(2)} = r\mathrm{d}\theta, \qquad (30)$$

$$e^{(3)} = \frac{\sqrt{\Delta}}{r^{3/4}(r^{3/2} - 3r^{1/2} + 2a)^{1/2}}[(r^{3/2} + a)\mathrm{d}\varphi - \mathrm{d}t], \quad (31)$$

which is a tetrad only on massive particle circular orbits in the equatorial plane. Then, the tetrad components of k^a at the source position are $k^{(\mu)} = k^a e^{(\mu)}{}_a|_{\theta = \pi/2}$, where

$$k^{(0)} = \frac{b - a - r^{3/2}}{r^{3/4}(r^{3/2} - 3r^{1/2} + 2a)^{1/2}}, \qquad (32)$$

$$k^{(1)} = \frac{\sigma_r}{r}\sqrt{\frac{R}{\Delta}}, \qquad (33)$$

$$k^{(2)} = \sigma_\theta \frac{\sqrt{q}}{r}, \qquad (34)$$
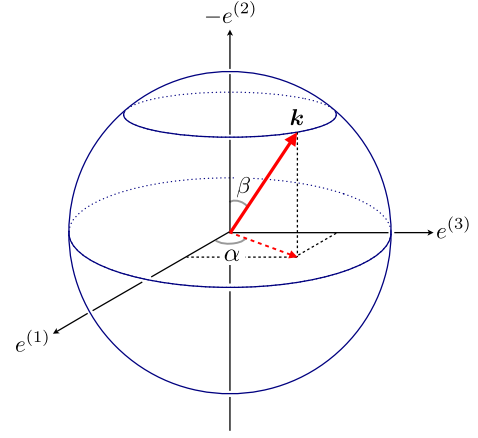
$$k^{(3)} = \frac{bE - L}{\sqrt{\Delta}}. \qquad (35)$$

FIG. 3. Definition of photon emission angles at a light source.

We parametrize the spatial direction of photon emission by two angle parameters (α, β) as follows:

$$\cos\alpha\sin\beta = \frac{k^{(1)}}{k^{(0)}}, \quad \cos\beta = -\frac{k^{(2)}}{k^{(0)}}, \quad \sin\alpha\sin\beta = \frac{k^{(3)}}{k^{(0)}}, \qquad (36)$$

where β is the polar angle measured from the direction $-e^{(2)}$ to the direction of $\boldsymbol{k}$ (projection of k^a normal to $e^{(0)}$), and α is the azimuthal angle measured from the direction $e^{(1)}$ to the projection of $\boldsymbol{k}$ on the plane spanned by $\{e^{(1)}, e^{(3)}\}$.[2] Figure 3 shows the relation between $\boldsymbol{k}$ and (α, β). Solving these relations for (α, β) and using the null condition, we have

$$\cos\alpha = \frac{k^{(1)}}{\sqrt{(k^{(1)})^2 + (k^{(3)})^2}}, \quad \sin\alpha = \frac{k^{(3)}}{\sqrt{(k^{(1)})^2 + (k^{(3)})^2}}, \qquad (38)$$

$$\cos\beta = -\frac{k^{(2)}}{k^{(0)}}, \quad \sin\beta = \frac{\sqrt{(k^{(1)})^2 + (k^{(3)})^2}}{k^{(0)}}. \qquad (39)$$

As a result, a pair (b, q) has a one-to-one relation to a pair of emission angles (α, β). Hence, the allowed parameter ranges of (b, q) for photon escape restrict the range of (α, β).

We now relate marginal parameter values for photon escape to (α, β). Let S be the complete set of emission angles (α, β) at which a photon can escape to infinity. We call S the escape cone of a photon. If a photon has emission

---

[2]The angles α and β are related to the directional cosines Ψ and Θ of a beam of radiation with respect to ϕ direction and θ direction in Ref. [17] as

$$\Theta = \beta, \qquad \cos\Psi = \sin\alpha\sin\beta. \qquad (37)$$

angles of the boundary values of S, it cannot escape to infinity anymore. We call the set of all critical emission angles ∂S; this set can be explicitly specified in terms of marginal parameter values given in Tables I and II as follows:

$$\partial S = \bigcup_{i=1,2} \{(\alpha_i, \beta_i) | 0 \leq q \leq 27\}, \quad (40)$$

where, in the extremal case, we have defined

$$(\alpha_1, \beta_1) \equiv (\alpha_{1(a)}, \beta_{1(a)}) \equiv (\alpha, \beta)|_{\sigma_r=-\atop b=2} \text{for } 0 \leq q < 3, \quad (41a)$$

$$(\alpha_1, \beta_1) \equiv (\alpha_{1(b)}, \beta_{1(b)}) \equiv (\alpha, \beta)|_{\sigma_r=-\atop b=b_1^s} \quad \text{for } 3 \leq q < f, \quad (41b)$$

$$(\alpha_1, \beta_1) \equiv (\alpha_{1(c)}, \beta_{1(c)}) \equiv (\alpha, \beta)|_{\sigma_r=+\atop b=b_1^s} \quad \text{for } f \leq q \leq 27, \quad (41c)$$

$$(\alpha_2, \beta_2) \equiv (\alpha, \beta)|_{\sigma_r=+\atop b=b_2^s} \quad \text{for } 0 \leq q \leq 27, \quad (42)$$

and in a subextremal case,

$$(\alpha_1, \beta_1) \equiv (\alpha_{1(b)}, \beta_{1(b)}) \equiv (\alpha, \beta)|_{\sigma_r=-\atop b=b_1^s} \quad \text{for } 0 \leq q < f, \quad (43a)$$

$$(\alpha_1, \beta_1) \equiv (\alpha_{1(c)}, \beta_{1(c)}) \equiv (\alpha, \beta)|_{\sigma_r=+\atop b=b_1^s} \quad \text{for } f \leq q \leq 27, \quad (43b)$$

$$(\alpha_2, \beta_2) \equiv (\alpha, \beta)|_{\sigma_r=+\atop b=b_2^s} \quad \text{for } 0 \leq q \leq 27. \quad (44)$$

Figure 4 shows the critical emission angles for photon escape. The red, green, blue, and orange lines show the critical angles $(\alpha_{1(a)}, \beta_{1(a)})$, $(\alpha_{1(b)}, \beta_{1(b)})$, $(\alpha_{1(c)}, \beta_{1(c)})$, and (α_2, β_2), respectively. Note that the region containing the coordinate origin bounded by critical angles corresponds to an escape cone. Figures 4(a)–4(c) show escape cones in the cases $r = 2.98$, 2.6, $r_I(= 2.32\ldots)$, respectively, for

(a) $a = 0.9$, $r = 2.98$

(b) $a = 0.9$, $r = 2.6$

(c) $a = 0.9$, $r = r_I \simeq 2.32$

(d) $a = 0.999$, $r = 2.98$

(e) $a = 0.999$, $r = 2$

(f) $a = 0.999$, $r = r_I \simeq 1.18$

(g) $a = 1$, $r = 2.98$

(h) $a = 1$, $r = 2$
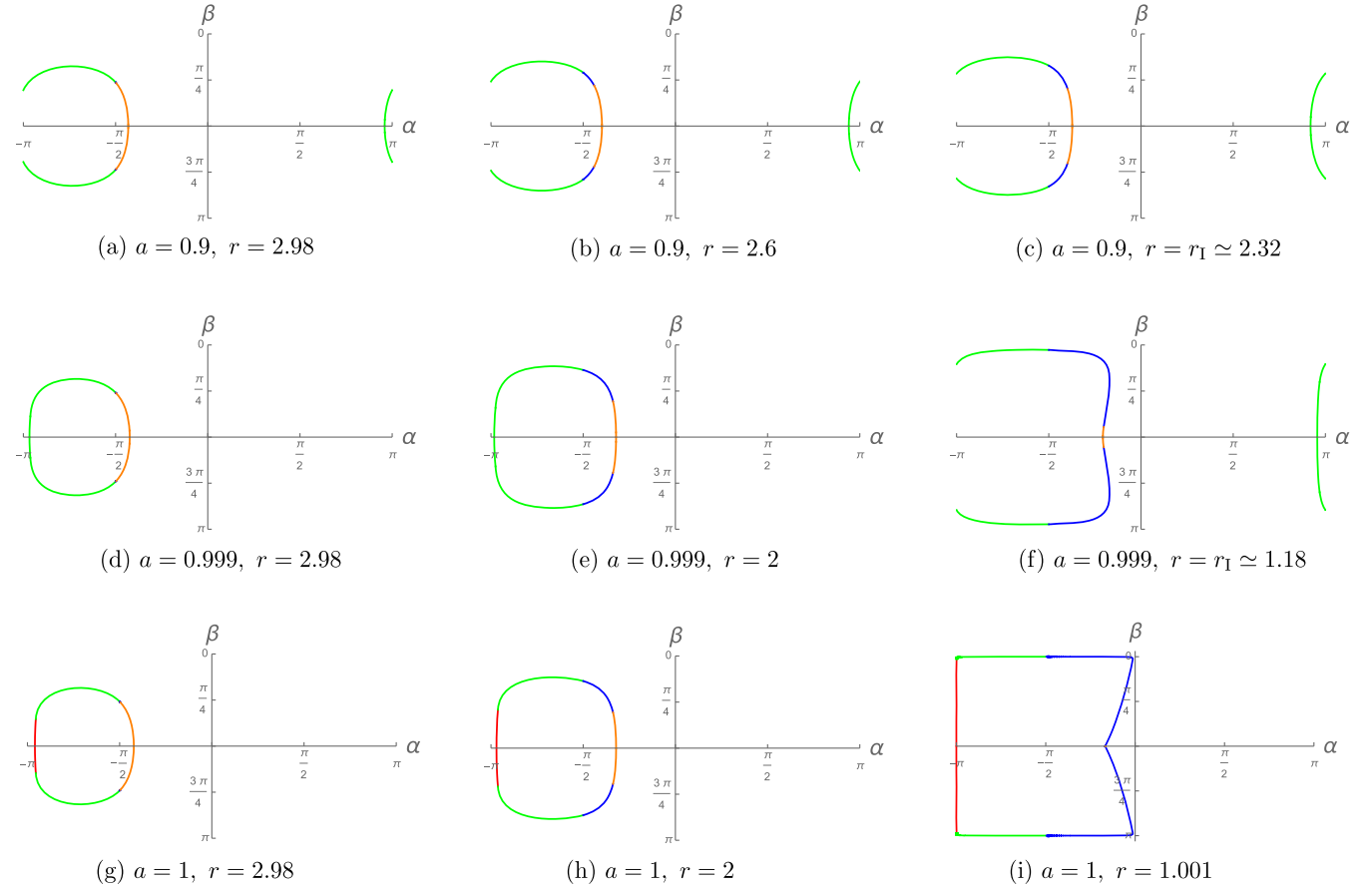
(i) $a = 1$, $r = 1.001$

FIG. 4. Escape cone of a photon emitted at a source circularly orbiting a rotating black hole. The first, second, and third lines show the cases $a = 0.9$, $a = 0.999$, and $a = 1$, respectively. The red, green, blue, and orange lines show $(\alpha_{1(a)}, \beta_{1(a)})$, $(\alpha_{1(b)}, \beta_{1(b)})$, $(\alpha_{1(c)}, \beta_{1(c)})$, and (α_2, β_2), respectively. The area containing the origin bounded by the colored lines corresponds to the escape cone of a photon.

$a = 0.9$. The horizon radius is $r_h \simeq 1.43\ldots$. The area of the escape cones becomes smaller as the emission point approaches the ISCO. Figures 4(d)–4(f) show escape cones in the cases $r = 2.98$, 2, $r_I(= 1.18\ldots)$, respectively, for $a = 0.999$. The horizon radius is $r_h = 1.04\ldots$. As is the case for $a = 0.9$, the area of the escape cones becomes smaller as r approaches the ISCO radius. Comparing photon emissions from the ISCO, we can see that the area of the escape cone in the case of $a = 0.999$ is smaller than that of $a = 0.9$. Figures 4(g)–4(i) show escape cones in the cases $r = 2.98$, 2, 1.001, respectively, for $a = 1$. The area of the escape cones becomes smaller as r decreases. It must be noted that, according to Fig. 4(i), even if the radial coordinate value of an emission point is sufficiently close to the horizon, $r = 1$, the escape cone still occupies over half of the unit sphere, indicating that more than half of the photons isotropically emitted from a circularly orbiting source can escape to infinity. In particular, as the entire region for which $0 \leq \alpha < \pi$ is included in the escape cone, all photons emitted forwardly from the source can escape to infinity.

We now assume that photon emission is isotropic and then evaluate the escape probability; this is identified with the solid angle of an escape cone divided by 4π, i.e.,

$$P = \frac{1}{4\pi} \int_S d\alpha d\beta \sin\beta. \tag{45}$$

In subextremal cases, in terms of critical angles, the escape probability P can be written as

$$P = 1 - \frac{1}{2\pi} \int_{r_I}^{r} dr_1 \frac{d\alpha_{1(b)}}{dr_1} \cos\beta_{1(b)}$$
$$- \frac{1}{2\pi} \int_{r}^{3} dr_1 \frac{d\alpha_{1(c)}}{dr_1} \cos\beta_{1(c)} - \frac{1}{2\pi} \int_{3}^{r_2^c} dr_2 \frac{d\alpha_2}{dr_2} \cos\beta_2. \tag{46}$$

All the integrands in the last three terms coincide with each other,

$$\left. \frac{d\alpha_{1(b)}}{dr_1} \cos\beta_{1(b)} \right|_{r_1=x} = \left. \frac{d\alpha_{1(c)}}{dr_1} \cos\beta_{1(c)} \right|_{r_1=x}$$
$$= \left. \frac{d\alpha_2}{dr_2} \cos\beta_2 \right|_{r_2=x} \equiv g(x). \tag{47}$$

Hence, we have

$$P = 1 - \frac{1}{2\pi} \int_{r_1^c}^{r_2^c} g(x) dx. \tag{48}$$

In the extremal case (i.e., $a = 1$), we can also write P in terms of critical angles as follows:

$$P = 1 - \frac{1}{2\pi} \int_{0}^{r_h} dr_1 \frac{d\alpha_{1(a)}}{dr_1} \cos\beta_{1(a)} - \frac{1}{2\pi} \int_{r_h}^{r_2^c} dx g(x). \tag{49}$$
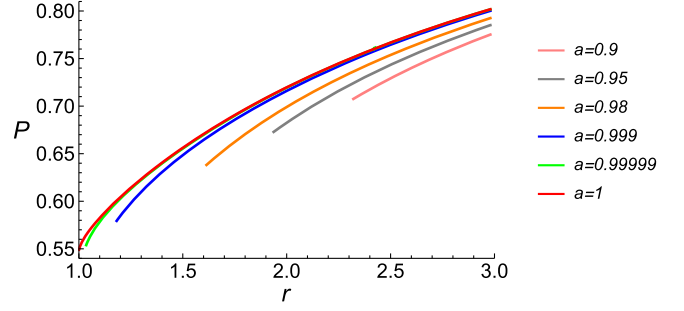

FIG. 5. Dependence of the escape probability P on the orbital radius r of a circularly orbiting source. The pink, gray, orange, blue, green, and red lines correspond to the cases $a = 0.9$, 0.95, 0.98, 0.999, 0.99999, and 1, respectively. The left end point on each line corresponds to ISCO for subextremal cases, and the left end point for $a = 1$ is $r = 1.001$.

Figure 5 shows the dependence of the photon escape probability P on the orbital radius r of a circularly orbiting source. The pink, gray, orange, blue, green, and red lines show the cases $a = 0.9$, 0.95, 0.98, 0.999, 0.99999, and 1, respectively. All P values decrease monotonically as r decreases toward r_I. Furthermore, the value of P evaluated at $r = r_I$ decreases monotonically as a approaches 1. For example, in the Thorne limit $a = 0.998$ [30], the value of P evaluated at the ISCO is

$$P(r_I) = 0.5880\ldots, \tag{50}$$

where $r_I = 1.236\ldots$. These results are consistent with a naive expectation that P becomes increasingly smaller as r approaches r_h. However, it is worth noting that $P(r_I)$ does not approach zero as a approaches 1. Even if a photon is emitted from the source circularly orbiting a near-extremal Kerr black hole with the orbital radius $r = r_I \simeq r_h$, the escape probability is about 55%. For the extremal case $a = 1$, in the limit as r approaches r_I (i.e., the horizon radius $r_I = r_h = 1$), P takes a nonzero value,

$$\lim_{r \to 1^+} P = 0.5464\ldots. \tag{51}$$

This indicates that more than half of photons emitted in the vicinity of the horizon escape to infinity without falling into the black hole.

We now evaluate the frequency shift of photons escaping from the ISCO to infinity. The redshift factor z measured by a static observer at infinity is given by

$$1 + z = -k^{(0)}. \tag{52}$$

Figures 6(a)–6(c) show the density contour of z for photons emitted from the front hemisphere of the source, which corresponds to the cases in Figs. 4(c), 4(f), and 4(i), respectively. The gray dashed lines show the contours of $z = 0$, and the red/blue regions show the emission angles
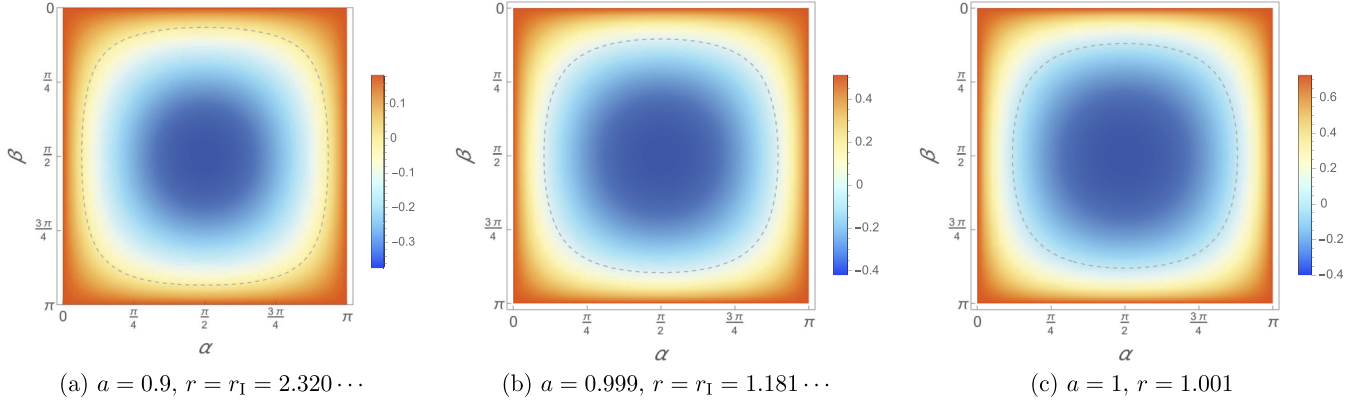
(a) $a = 0.9$, $r = r_\mathrm{I} = 2.320\cdots$ (b) $a = 0.999$, $r = r_\mathrm{I} = 1.181\cdots$ (c) $a = 1$, $r = 1.001$

FIG. 6.   Density contour plot of the redshift factor z in the ranges $0 \leq \alpha \leq \pi$ and $0 \leq \beta \leq \pi$ (i.e., front side emission). The gray dashed lines indicate the contour $z = 0$. The red and blue regions denote redshift and blueshift, respectively.

with which a photon is redshifted/blueshifted. The redshift factor is determined by the competition between the gravitational redshift and the Doppler blueshift. As a increases, the emission angles indicating blueshift decrease, but more than half of the hemisphere still shows blueshift.[3] We interpret that the Doppler blueshift due to the proper motion of the source overcomes the gravitational redshift. Therefore, combined with the escape probability results, this implies that photons escaping from the vicinity of the black hole horizon certainly transport the information of the near-horizon region and relativistic phenomena to distant observers.

IV. SUMMARY AND DISCUSSIONS

We have considered the observability of an isotropically emitting point source on a circular orbit near the horizon of a rapidly rotating black hole. When the source in a circular orbit loses energy and angular momentum, it eventually reaches the ISCO. Because the ISCO radius is very close to the horizon radius in a near-extremal Kerr spacetime, the observability of the ISCO indicates that of the near-horizon region and is essential for distinguishing whether or not the central object is a black hole.

We have provided a method to calculate the escape cone of a photon emitted from the source and shown it explicitly; our results indicate that a photon emitted forward and outward from the source is likely to escape to infinity, while one emitted backward and inward is likely to fall into the horizon. On the basis of these results, we have evaluated the escape probability of a photon as a function of the orbital radius of the circularly orbiting source. As a result, we have found that it decreases monotonically as the radius approaches the ISCO. Furthermore, we have shown that the

escape probability evaluated at the ISCO decreases monotonically when the Kerr parameter approaches the extremal value. Despite the fact that the ISCO radius eventually coincides with the horizon radius in the extremal case [26,27], the probability does not become zero even in the limit of the ISCO; on the contrary, it remains at 54.6%. In a near-extremal Kerr spacetime, the ISCO radius is always larger than the innermost spherical photon orbit radius (i.e., unstable circular orbit radius). This fact implies that a photon emitted inward from the ISCO can be bounced back at a turning point by a potential barrier if it has a specific impact parameter. In the extremal Kerr spacetime, a photon can have a turning point arbitrarily close to the horizon. Hence, photons can be scattered despite being emitted inward from a region very close to the horizon. This is why the escape probability becomes nonzero (or has nonzero measure) in the ISCO limit of the (near) extremal Kerr. We leave a more clear explanation of relatively large escape probability by the extremal Kerr throat geometry as future work. Because the value of 54.6% is larger than 29.1%—the escape probability of a photon emitted from the locally nonrotating source in the limit as the source approaches the horizon [12]—we can interpret this enhancement as the result of the boost (or the relativistic beaming) due to the circular motion of the source. We have also found that photons emitted from the front side of the source get blueshifted for distant observers, i.e., the Doppler blueshift due to the proper motion of the source can overcome the gravitational redshift.

On the basis of these results, we conclude that the ISCO of a rapidly rotating black hole spacetime is observable. Our results provide insight into optical phenomena such as the observation of a black hole shadow. The ISCO is often identified as the innermost edge of the accretion disk or is considered as the position where the phase of accretion flow switches; however, in any case, the orbit is located in the immediate vicinity of the near-extremal rotating black hole. Photons emitted from this region contain information on the near-horizon region and phenomena, and certainly transport

---

[3]In the extremal Kerr geometry, it is known that z varies smoothly with the directional cosine Ψ with respect to ϕ direction, and there always exists the range of Ψ where z shows a net blueshift [17].

it to infinity. Finally, the information can be obtained from photons that appear as the edge of the black hole shadow to a distant observer. From this, we can conclude that if a black hole is rapidly spinning, signs of near-horizon physics will be detectable on the edge of the shadow.

ACKNOWLEDGMENTS

[1] K. Akiyama *et al.* (Event Horizon Telescope Collaboration), First M87 Event Horizon Telescope results. I. The shadow of the supermassive black hole, Astrophys. J. **875,** L1 (2019).

[2] K. Akiyama *et al.* (Event Horizon Telescope Collaboration), First M87 Event Horizon Telescope results. II. Array and instrumentation, Astrophys. J. **875,** L2 (2019).

[3] K. Akiyama *et al.* (Event Horizon Telescope Collaboration), First M87 Event Horizon Telescope results. III. Data processing and calibration, Astrophys. J. **875,** L3 (2019).

[4] K. Akiyama *et al.* (Event Horizon Telescope Collaboration), First M87 Event Horizon Telescope results. IV. Imaging the central supermassive black hole, Astrophys. J. **875,** L4 (2019).

[5] K. Akiyama *et al.* (Event Horizon Telescope Collaboration), First M87 Event Horizon Telescope results. V. Physical origin of the asymmetric ring, Astrophys. J. **875,** L5 (2019).

[6] K. Akiyama *et al.* (Event Horizon Telescope Collaboration), First M87 Event Horizon Telescope results. VI. The shadow and mass of the central black hole, Astrophys. J. **875,** L6 (2019).

[7] Y. Mizuno, Z. Younsi, C. M. Fromm, O. Porth, M. De Laurentis, H. Olivares, H. Falcke, M. Kramer, and L. Rezzolla, The current ability to test theories of gravity with black hole shadows, Nat. Astron. **2,** 585 (2018).

[8] V. Cardoso and P. Pani, Testing the nature of dark compact objects: A status report, Living Rev. Relativity **22,** 4 (2019).

[9] A. Lupsasca, A. P. Porfyriadis, and Y. Shi, Critical emission from a high-spin black hole, Phys. Rev. D **97,** 064017 (2018).

[10] T. Igata, H. Ishihara, and Y. Yasunishi, Observability of spherical photon orbits in near-extremal Kerr black holes, Phys. Rev. D **100,** 044058 (2019).

[11] K. Ogasawara, T. Harada, U. Miyamoto, and T. Igata, Escape probability of the super-Penrose process, Phys. Rev. D **95,** 124019 (2017).

[12] K. Ogasawara, T. Igata, T. Harada, and U. Miyamoto, Escape probability of a photon emitted near the black hole horizon, Phys. Rev. D **101,** 044023 (2020).

[13] R. Takahashi and M. Takahashi, Anisotropic radiation field and trapped photons around the Kerr black hole, Astron. Astrophys. **513,** A77 (2010).

[14] S. S. Doeleman *et al.*, Jet launching structure resolved near the supermassive black hole in M87, Science **338,** 355 (2012).

[15] Y. R. Li, Y.-F. Yuan, J.-M. Wang, J.-C. Wang, and S. Zhang, Spins of supermassive black holes in M87. II. Fully general relativistic calculations, Astrophys. J. **699,** 513 (2009).

[16] J. Feng and Q. Wu, Constraint on the black-hole spin of M87 from the accretion-jet model, Mon. Not. R. Astron. Soc. **470,** 612 (2017).

[17] C. T. Cunningham and J. M. Bardeen, The optical appearance of a star orbiting an extreme Kerr black hole, Astrophys. J. **183,** 237 (1973).

[18] C. T. Cunningham, The effects of redshifts and focusing on the spectrum of an accretion disk around a Kerr black hole, Astrophys. J. **202,** 788 (1975).

[19] J. P. Luminet, Image of a spherical black hole with thin accretion disk, Astron. Astrophys. **75,** 228 (1979).

[20] J. Fukue and T. Yokoyama, Color photographs of an accretion disk around a black hole, Publ. Astron. Soc. Jpn. **40,** 15 (1988).

[21] H. Falcke, F. Melia, and E. Agol, Viewing the shadow of the black hole at the galactic center, Astrophys. J. **528,** L13 (2000).

[22] R. Takahashi, Shapes and positions of black hole shadows in accretion disks and spin parameters of black holes, J. Korean Phys. Soc. **45,** S1808 (2004); Astrophys. J. **611,** 996 (2004).

[23] T. Kawashima, M. Kino, and K. Akiyama, Black hole spin signature in the black hole shadow of M87 in the flaring state, Astrophys. J. **878,** 27 (2019).

[24] S. E. Gralla and A. Lupsasca, Lensing by Kerr black holes, Phys. Rev. D **101,** 044031 (2020).

[25] I. D. Novikov and K. S. Thorne, Astrophysics of black holes, in *Black Holes (Les Astres Occus)*, edited by C. DeWitte and B. DeWitt (Gordon and Breach, New York, 1973), p. 343.

[26] J. M. Bardeen, W. H. Press, and S. A. Teukolsky, Rotating black holes: Locally nonrotating frames, energy extraction, and scalar synchrotron radiation, Astrophys. J. **178,** 347 (1972).

[27] D. Kapec and A. Lupsasca, Particle motion near high-spin black holes, Classical Quantum Gravity **37,** 015006 (2020).

[28] S. E. Gralla, A. P. Porfyriadis, and N. Warburton, Particle on the innermost stable circular orbit of a rapidly spinning black hole, Phys. Rev. D **92,** 064029 (2015).

[29] S. E. Gralla, A. Lupsasca, and A. Strominger, Observational signature of high spin at the Event Horizon Telescope, Mon. Not. R. Astron. Soc. **475,** 3829 (2018).

[30] K. S. Thorne, Disk accretion onto a black hole. II. Evolution of the hole, Astrophys. J. **191,** 507 (1974).